HHS Public Access

Author manuscript

Cancer Res. Author manuscript; available in PMC 2021 March 15.

Published in final edited form as:

Cancer Res. 2020 September 15; 80(18): 3841–3854. doi:10.1158/0008-5472.CAN-20-1744.

BRG1 loss predisposes lung cancers to replicative stress and ATR dependency

Manav Gupta[1], **Carla P. Concepcion**[2], **Caroline G. Fahey**[1], **Hasmik Keshishian**[3], **Arjun Bhutkar**[2], **Christine F. Brainson**[1,8], **Francisco J. Sanchez-Rivera**[2,9], **Patrizia Pessina**[1], **Jonathan Y. Kim**[2], **Antoine Simoneau**[4], **Margherita Paschini**[1], **Mary C. Beytagh**[2], **Caroline R. Stanclift**[3], **Monica Schenone**[3,10], **D R. Mani**[3], **Chendi Li**[6], **Audris Oh**[6], **Fei Li**[5], **Hai Hu**[5], **Angeliki Karatza**[5], **Roderick T. Bronson**[7], **Alice T. Shaw**[6,11], **Aaron N. Hata**[6], **Kwok-Kin Wong**[5], **Lee Zou**[4], **Steven A. Carr**[3], **Tyler Jacks**[2], **Carla F. Kim**[1,*]

[1,]Stem Cell Program, Division of Hematology/Oncology and Division of Respiratory Disease, Boston Children's Hospital, Boston, MA 02115, USA; Department of Genetics, Harvard Medical School, Boston, MA 02115, USA; Harvard Stem Cell Institute, Cambridge, MA 02138, USA.

[2,]David H. Koch Institute for Integrative Cancer Research, Massachusetts Institute of Technology, 500 Main Street, Cambridge, MA 02139, USA; Department of Biology, Massachusetts Institute of Technology, 77 Massachusetts Avenue, Cambridge, MA 02139, USA; Howard Hughes Medical Institute, Massachusetts Institute of Technology, Cambridge, MA 02139, USA.

[3,]Broad Institute of MIT and Harvard, 415 Main St, Cambridge, MA 02142

[*]Corresponding author. Ph – 617-919-4644, carla.kim@childrens.harvard.edu.

Author contributions

M.G., C.P.C., K.K.W., A.N.H., S.A.C., L.Z., T.J., and C.F.K. designed the study;
M.G. C.P.C., C.G.F., C.F.B., F.J.S-R., P.P., A.B, M.P. J.Y.K., H.K., C.R.S., M.S., D.R.M performed the experiments;
H.K., C.R.S., M.S., D.R.M, S.A.C performed mass spectrometry and analysis;
A.S., L.Z., helped with DNA fibers experiments;
R.T.B provided expertise on understanding tumor development in xenograft assays;
M.C.B, F.L., H.H., A.K., helped make in vitro models of Brg1 loss;
C.L, A.O generated the PDX-derived cell lines;
A.T.S., A.N.H. provided PDX models and clinical information;
M.G. and C.F.K. wrote the manuscript with comments from all authors

Competing interests

C.F.K has a sponsored research agreement from Celgene/BMS and Dutch Lung Foundation, but this funding did not support the research described in this manuscript. C.F.K has received honorarium from MedImmune (AstraZeneca), Genentech, The Rockefeller University, and American Thoracic Society.

T.J. is a member of the Board of Directors of Amgen and Thermo Fisher Scientific. He is also a co-Founder of Dragonfly Therapeutics and T2 Biosystems. T.J. serves on the Scientific Advisory Board of Dragonfly Therapeutics, SQZ Biotech, and Skyhawk Therapeutics. None of these affiliations represent a conflict of interest with respect to the design or execution of this study or interpretation of data presented in this manuscript. T.J. laboratory currently also receives funding from the Johnson & Johnson Lung Cancer Initiative and The Lustgarten Foundation for Pancreatic Cancer Research, but this funding did not support the research described in this manuscript.

L.Z. has consulted for EMD Serono and received research funding from Calico.

S.A.C. is a member of the scientific advisory boards of Kymera, PTM BioLabs and Seer and a scientific advisor to Pfizer and Biogen.

A.N.H has received research funding from Amgen, Pfizer, Eli Lilly, Roche/Genentech, Relay Therapeutics and Novartis.

A.T.S has served as a compensated consultant or received honoraria from Achilles, Archer, ARIAD, Bayer, Blueprint Medicines, Chugai, Daiichi Sankyo, EMD Serono, Foundation Medicine, Genentech/Roche, Guardant, Ignyta, KSQ Therapeutics, LOXO, Natera, Novartis, Pfizer, Servier, Syros, Taiho Pharmaceutical, Takeda and TP Therapeutics; has received research (institutional) funding from Daiichi Sankyo, Ignyta, Novartis, Pfizer, Roche/Genentech and TP Therapeutics; has served on the Board of Directors of Syros Pharmaceuticals; and is currently an employee of Novartis.

K.K.W. is a founder and equity holder of G1 Therapeutics and he has consulting/sponsored research agreements with AstraZeneca, Janssen, Pfizer, Array, Novartis, Merck, Takeda, Ono, Targimmune, and BMS.

[4]Department of Pathology, Massachusetts General Hospital, Harvard Medical School, Boston, MA 02115, USA. Massachusetts General Hospital Cancer Center, Harvard Medical School, Charlestown, MA 02129, USA.

[5]Laura and Isaac Perlmutter Cancer Center, New York University Grossman School of Medicine, NYU Langone Health, New York, NY 10016, USA.

[6]Massachusetts General Hospital Cancer Center and Department of Medicine Massachusetts General Hospital Harvard Medical School, Boston, MA, 02115, USA

[7]Department of Microbiology and Immunobiology, Harvard Medical School MA 02115, USA

[8]Markey Cancer Center, University of Kentucky, Lexington, KY, USA; Department of Toxicology and Cancer Biology, University of Kentucky, Lexington, KY 40536 USA (current address)

[9]Cancer Biology and Genetics Program, Memorial Sloan Kettering Cancer Center, New York, NY 10065, USA (current address)

[10]Pfizer Cambridge Labs, 1 Portland St, MA 02139 (current address)

[11]Novartis Institutes of Biomedical Research, Cambridge, MA 02139, USA (current address)

Abstract

Inactivation of SMARCA4/BRG1, the core ATPase subunit of mammalian SWI/SNF complexes, occurs at very high frequencies in non-small cell lung cancers. There are no targeted therapies for this subset of lung cancers, nor is it known how mutations in BRG1 contribute to lung cancer progression. Using a combination of gain- and loss-of-function approaches, we demonstrate that deletion of BRG1 in lung cancer leads to activation of replication stress responses. Single-molecule assessment of replication fork dynamics in BRG1-deficient cells revealed increased origin firing mediated by the pre-licensing protein CDC6. Quantitative mass spectrometry and co-immunoprecipitation assays showed that BRG1-containing SWI/SNF complexes interact with RPA complexes. Lastly, BRG1-deficient lung cancers were sensitive to pharmacological inhibition of ATR. These findings provide novel mechanistic insight into BRG1-mutant lung cancers and suggest that their dependency on ATR can be leveraged therapeutically and potentially expanded to BRG1-mutant cancers in other tissues.

Graphical Abstract

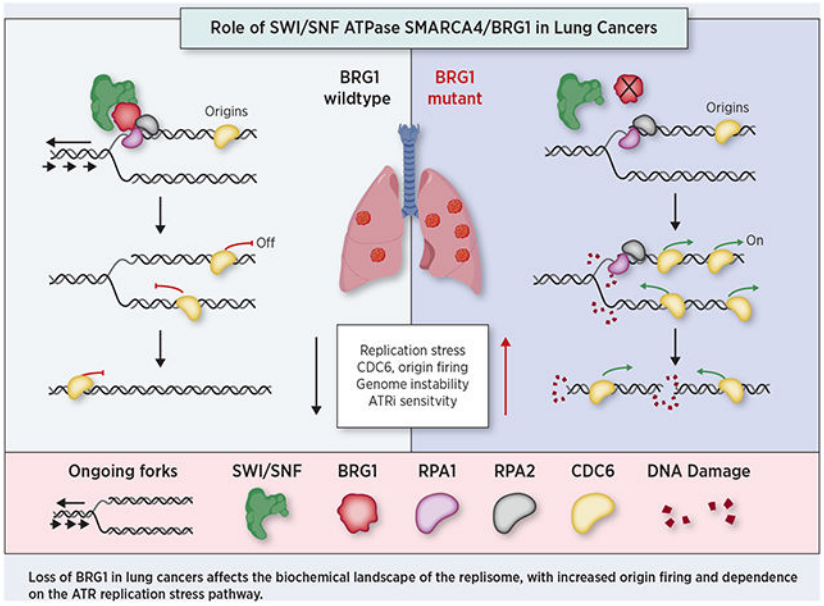

Loss of BRG1 in lung cancers affects the biochemical landscape of the replisome, with increased origin firing and dependence on the ATR replication stress pathway.

Introduction

Lung cancer remains the leading cause of cancer related mortality worldwide (1). While genotype-specific treatments for EGFR, ROS1, and ALK have transformed the landscape of precision medicine in lung cancer patients, the ability to stratify patients has not yet led to targeted therapies for patients whose tumors bear other frequent mutations (2). The mammalian SWI/SNF complexes, also known as BRG1/BRM associated factors (BAF) complexes (referred to hereafter as SWI/SNF) are multi-subunit protein complexes that use ATP-dependent processes to mobilize nucleosomes to modulate gene expression and are mutated in many cancer types (3–8). Mutations in *SMARCA4/BRG1*, the ATPase core of SWI/SNF chromatin remodeling complexes, have been found to be prevalent at a high frequency in lung cancer (9–12). Furthermore, the genomic location of *BRG1* on chromosome 19p13.2 along with key lung cancer genes *KEAP1* and *STK11*, has been associated with loss of heterozygosity events that compound the cases of *BRG1* mutations with those which sustain whole chromosome arm deletions and subsequent inactivation (13). In a recent study in which *BRG1* mutations were found in 10% of non-small cell lung cancers (NSCLC), mutations in *BRG1* commonly occurred with other well-known lung cancer mutations in *KRAS, TP53* (14). Clinical outcomes in patients with *BRG1*-mutant lung cancer were poor and showed limited efficacy with standard-of-care treatments (14). Thus, the current understanding of this genotype in lung cancer patients remains limited, from both a mechanistic and a clinical standpoint.

Functionally, monoallelic or biallelic inactivation of *Brg1* during murine embryogenesis leads to tumors or preimplantation lethality respectively, but certain tissue types including the lung acquire frequent *BRG1* mutations during tumorigenesis (15). Moreover, targeted deletion of *Brg1* in carcinogen-induced lung cancer models has been shown to enhance lung cancer progression and promote metastasis (16, 17). Also notable is the fact that, genetically engineered murine models (GEMM) of lung adenocarcinoma (LUAD) spontaneously show

loss of *Brg1* focal regions as one of the foremost changes to the murine LUAD progression landscape (18). At the molecular level, the presence of Brg1 in murine embryonic stem cells promoted decatenation of newly replicated sister chromatids to allow for faithful replication through mitosis (19). This function was dependent on the ability of Brg1 to recruit topoisomerases to resolve torsional stress in entangled DNA. In murine fibroblasts, loss of Brg1 resulted in aberrant mitosis, linked to its chromatin modifying properties of heterochromatin states (20). Biochemical interactions between Brg1 and Topbp1 was recovered in murine fetal liver cells, suggesting roles for Brg1 during S-phase (21). In BRG1-deficient cancer lines, loss of biochemical interactions between BRG1 and retinoblastoma have been linked to uncontrolled proliferation mediated by increased expression of E2F target genes (22). Thus, whereas studies have implicated BRG1 as either a transcriptional regulator during G1/S or as a substrate that promotes specific interactions through mitosis, the effects of BRG1 loss on DNA replication during cancer progression is unknown. In the present study, we sought to address unanswered questions about the mechanistic implications of BRG1 loss of function in lung cancers that could be clinically relevant.

Materials and Methods

Human cell lines.

Human lung cancer cell lines used in this study include H460, H2009, Calu6, H441, Sw1573, Calu3, HCC827, Calu1, H520, A549, H522, H2030, H1299, H2126, H157. All cell lines were maintained in RPMI 1640 media (Invitrogen 11875–119) with 10% fetal bovine serum (Fisher 35–016-CV), 4mM L-glutamine (Life Technologies 25030–164) and penicillin/streptomycin (Life Technologies 15140122) at 37°C, 5% CO2. Cell lines were obtained from the Meyerson laboratory. Cell cultures were routinely tested for and were negative for mycoplasma. Frozen stocks were made for all cell lines and experiments were performed within first few passages after each thaw. KRAS-mutant lung adenocarcinoma PDX-derived cell lines were provided by the Hata laboratory.

Murine cell lines and gene-editing.

Polyclonal Kras/p53 cell lines (23) generated from C57BL/6J mice (Jackson Laboratory) were used for generation of isogeneic *Brg1* knockout lines. Cell lines were nucleofected with pX458 (24) vector encoding Cas9, GFP and a guide against the tomato gene (25) or *Brg1*. Cells were sorted to single cells in 96 well plate after gating on GFP-positive cells. Clones were expanded and screened by western Blot for Brg1 expression. Lines with reduced expression were then sequence confirmed by Topo cloning.

Human cell lines and gene-editing.

Selected guides, *sgTom* control and *sgBRG1*, were cloned into the pLentiCRISPR vector (26), which was used to produce lentivirus using established protocols (27). H460, H2009, and Calu6 were infected and after puromycin selection, single cell clones were generated and verified by western blot. Clones with BRG1 loss were then sequence confirmed by Topo cloning. Guide sequences: *sgTom* ccatcgatctcgaactcgtggcc, *sgBRG1* ccacgtggagagtgggaagatcc, *sgBrg1* ccacgtggagagtggcaagatcc. The BRG1 overexpression

plasmid (#19148) from the Massague laboratory (28) was purchased through Addgene. For BRG1 overexpression experiments, retroviruses were generated and packaged in PlatE cells using established protocols (29). Cell lines were infected with viral containing supernatant containing 8 μg/ml polybrene (Sigma TR-1003-G) for a period of 10–18 h. Infected cultures were selected with hygromycin (Invitrogen 10687–010) 5 days after infection.

Drugs.

DMSO (Sigma D2438–5X10ML), KU-60019 (Selleck KU-60019), MK-8776 (Selleck S2735), Irinotecan (Selleck S2217), Olaparib (Selleck S1060), VX-680 (Selleck S1048), Palbociclib (Selleck S1116), VX-970 (Cayman Chemical Co 24198), Hydroxyurea (Sigma H8627–5G). Pemetrexed and Carboplatin were provided by the Wong lab.

Cytotoxicity assays.

Cell viability assays were performed with Cell-Titer Glo (Promega G7572), as previously described (30). For human dose-dependent experiments, the following doses were used: 0, 0.1, 0.3, 0.5, 0.7, 1, 3, 5, 7, 10, 50 μM; for murine experiments VX-970 was used at: 0, 0.1, 0.5, 1, 5, 10 μM. Combination experiments with irinotecan and hydroxyurea were performed at 1μM and 1mM, respectively. Following 72 hours of incubation, Cell-Titer Glo was added per well for 10–15 minutes and ATP-based luminescence was measured on a BioTec plate reader. Data were averaged over triplicates and normalized to control (DMSO/water) treated wells. Log (IC50) and S.E.M. values were compared using GraphPad Prism software, and p-values reported were the sum-of-squares F-statistics.

Cell cycle.

Cell cycle profiles of human cell lines were determined by BrdU pulse followed by flow cytometry analysis for BrdU/7-AAD positive cycling cells. Briefly, cells were pulsed with 10μM BrdU for 1–2 hours, and followed by overnight fixation in 100% ethanol. Cells were stained with BrdU-FITC (BD556028) and 7-AAD for DNA and analyzed by flow cytometry. Murine cell cycle profiles were determined using the APC BrdU Flow Kit (BD552598) as per manufacturer's instructions. Asynchronous cell cycle experiments were performed as described before. All flow cytometry was performed on the BD Fortessa machine. Data was subsequently analyzed on FlowJo software and S-phase lengths were determined based on peak intensity of EdU staining at appropriate time point.

Western Blot.

Protein was taken from whole-cell extracts made in RIPA buffer (0.5% Deoxycholate, 1% CA630, 0.1% sodium dodecyl sulphate, 150 mM NaCl, 50 mM Tris-8.1). Samples were quantified using the Pierce 660 nm Protein Assay Kit (Thermo Fisher 22662). Each sample was denatured in 2x Laemmli buffer (BioRad 1610737) at 95C for 10 minutes. Samples were run on a 4–15% polyacrylamide gel (BioRad 456–1086) and transferred onto a nitrocellulose membrane (GE Healthcare 45-004-003) via wet transfer for 1 hour. Membranes were incubated overnight at 4C in primary antibody. Anti-HRP (Santa Cruz) secondary antibodies were diluted 1:2000. ECL-based methods (Perkin Elmer NEL103001EA) was used to visualize the on KODAK BioMax XAR film (Sigma Z370371–

50EA). The following antibodies were used in this study. CST antibodies – ATR (2790S), CHK1 (2360S), pCHK1 (2341S), Histone H3 (4499S), BAF155 (11956S), BAF170 (12760S), ARID1A (12354S), CDC6 (3387T), ORC1 (4731T), RPA1 (2267S), RPA2 (52448S), BAF47 (91735S), LKB1 (3047S), KEAP1 (8047S). TOPBP1 was purchased from Bethyl (8047S).

Immunoprecipitation.

Cell pellets were washed in cold 1x PBS, and resuspended in 50/100 μL RIPA buffer (0.5% deoxycholate, 1% CA630, 0.1% sodium dodecyl sulphate, 150 mM NaCl, 50 mM Tris-8.1) with protease (Roche 11836170001) and phosphatase inhibitors (Fisher PIA32957). The samples were lysed on ice for 30 minutes, vortexed every 10 minutes. The lysates were then centrifuged for 30 minutes at 4C at 14,000g. 100–200 μg of lysates were pre-cleared with specific antibody for 25 minutes by rotation at 4C. Protein A agarose beads (Thermo Fisher 10001D) were washed three times in 1 mL RIPA buffer. Approximately 70 μL of beads were added to each protein-antibody sample and rotated overnight at 4C. Samples were then spun down at 2,300 × g for 2 minutes, washed with 1 mL RIPA buffer, rotated for 3 minutes at 4C three times, followed by western blot.

RNA-sequencing.

Bulk RNA-sequencing was performed in triplicates for murine isogenic cells. Bulk RNA-seq reads that passed quality metrics were mapped to the annotated UCSC mm9 mouse genome build (genome.ucsc.edu) using RSEM (v1.2.12) (deweylab.github.io/RSEM) (31) using RSEM's default Bowtie (v1.0.1) alignment program (32). RSEM estimated read counts were used to perform pairwise differential gene expression analysis between experimental conditions using EBSeq (33) with median-by-ratio normalization (34). Mouse gene symbols were updated to their most-recent nomenclature using data from the Mouse Genome Informatics (MGI) batch query utility (www.informatics.jax.org/batch) and subsequently mapped to orthologous human gene symbols using mouse-human ortholog assignments (www.informatics.jax.org/downloads/reports/index.html) from MGI (35). Ranked gene lists by fold change were analyzed through a pre-ranked gene set enrichment analysis (GSEA) algorithm against Gene Ontology (GO) and Reactome databases using MsigDB (36, 37), using default conditions. Normalized enrichment scores ("Enrichment Score") for GO categories and Reactome pathways were used to generate dot plots.

Kaplan-Meier plots.

Survival analysis in lung cancer patients was performed on KM plotter (https://kmplot.com/analysis/) (38). Kaplan–Meier survival analyses were implemented for NSCLC patients (LUAD, n = 866; LSCC, n = 675) using median gene expression values to split patient group. Cox regression analysis was performed to compute hazard ratios with 95% confidence intervals and logrank p-values. Survival differences between the two risk groups were assessed using the Mantel–Haenszel log-rank test.

Xenografts.

1 million cells were injected subcutaneously into the flanks of 8–12-week-old female Foxn1nu/Foxn1nu mice (Jackson Laboratory) in a 1:1 ratio with matrigel. Each mouse received either BRG1 wildtype or knockout cells on the right and left flank, respectively. Following the establishment of visible tumors, mice were randomized for treatment studies. VX-970 was administered from day 7–14 at a dose of 60mg/kg/d in 5% DMSO + 45% PEG300 (Sigma 57668–5G) + H_2O once per day for 5 consecutive days by oral gavage. Treatments lasted between 25–30 days. Tumor growth was measured every 4 days by caliper in a non-blinded fashion. Subcutaneous tumor volumes were calculated according to the following formula: volume (mm3) = (l × b × h) × (π/6), where l is the largest dimension followed by b and h. All mouse experiments performed at BCH were approved by the Animal Care and Use Committee accredited by the Association for Assessment and Accreditation of Laboratory Animal Care and were performed in accordance with relevant institutional and national guidelines and regulations.

Immunofluorescence.

Cells were prefixed in 4% paraformaldehyde and antigen unmasking was performed using citrate buffer (Thermo Fisher TA-250-PM1X). Cells were blocked in 10% donkey serum in 0.2% Triton X-100 in PBS and probed with primary antibodies overnight at 4C. Following washes and incubation with secondary antibodies, slides were mounted using Prolong Gold with DAPI (Life Technologies P36935). Images were taken with a Nikon 90i camera and NIS-Elements software. For gamma-H2AX and RPA2 experiments, cells were pre-extracted with 0.1% Triton X-100 in PBS for 2 minutes on ice before fixation. For DNA fibers, fiber slides were treated with 2.5M HCl for 30 minutes and blocked in 3% BSA/PBST (PBS + 0.05% Tween20) for 1 hour. Primary antibody incubation was performed for 1 hour with anti-CIdU (Novus NB 500–169, 1:100) and anti-IdU (BD-347580, 1:20). Following 3 washes with PBS, fibers were stained with appropriate secondary antibodies for 30 minutes and finally washed, dried and mounted with Prolong Gold without DAPI (Life Technologies P36934). Slides were dried overnight at room temperature in the dark, and then stored at 4C until imaging.

Comets.

Alkaline comet electrophoresis was performed based on manufacturer’s instructions (Trevigen). Briefly, cells were trypsinized, collected in cold 1x PBS, and mixed in 1:10 ratio with low melting agarose (Bio-Rad 1613111). 30μl of cells/agarose was pipetted and spread gently on a comet slide (Trevigen 4252-200-01). Following a 10-minute incubation in the dark at 4C, the comet slides were submerged in lysis solution (Trevigen 4250-050-01) for overnight incubation at 4C in the dark. The next day, the slides were incubated in alkali unwinding solution for 60 minutes at 4C and run in an electrophoresis unit at 17 volts for 34 minutes. Following washes with 70% ethanol and distilled water, slides were allowed to naturally dry in a 37C incubator, before proceeding to staining with SyBr Gold nucleic acid stain (Thermo Fisher S11494).

DNA fibers.

DNA fibers were performed in accordance to published protocols (39). Briefly, cells were sequentially pulsed with 50μM CIdU (Sigma C6891) and 100μM IdU (Sigma 17125) with PBS washes in between. Cells were then trypsinized and resuspended at a dilution of 1 million cells per ml. 2.5μl of were pipetted on the top of a glass slide. Following an approximate 4-minute incubation, 7.5μl spreading buffer (0.5% SDS, 200mM Tris-HCl pH 7.4, 50mM EDTA, water) was mixed with the cells and allowed to incubate for 2 minutes. 3 glass slides were made per condition per experiment. Slides were tilted at 15 degrees to allow DNA fibers to evenly spread on the glass slide. Following that, the fibers were air dried and then fixed in 3:1 methanol: acetic acid solution. Fixed slides were allowed to dry for 20 minutes and then stored at 4C until immunofluorescence. Measurement of replication structures was performed using Image J. A total of 150–200 definitively resolved fibers were quantified per condition per replicate and the percentage of each specific replication structure was calculated based on total counts observed.

Mass spectrometry.

Murine isogenic cells were scraped in ice-cold PBS, washed twice, and lysed with mild lysis buffer (150 mM NaCl, 50 mM Tris pH 7.5, 1% IGEPAL-CA-630 with protease inhibitors) on ice for 30 mins. Lysates were treated with MNase with calcium chloride for 4 mins at 28C. MNase digestion was halted with EGTA. Lysates were then spun at top speed at 4C using a microcentrifuge followed by protein quantification through BCA. Samples were diluted with lysis buffer to 1 mg/ml. 60 ug of antibody (anti-BAF47 or isotype control) was added to 1 mg of lysate (2 process replicates per condition) and incubated overnight at 4C, rotating. The following day, Protein G beads (Life Technologies 10003D) were washed 1X with lysis buffer, resuspended with lysate, and rotated at 4C for 4 hours. Beads were then washed 3X with wash buffer (150 mM NaCl, 50 mM Tris pH 7.5 with protease inhibitors) and submitted for proteomics analysis. Sample processing for mass spectrometry analysis was performed as described previously (40). Briefly, on bead digestion of samples was performed for 1 hour followed by elution of samples from the beads, reduction, alkylation and overnight digestion of the supernatant with trypsin. Digested peptides were labeled using eight channels of tandem mass tag (TMT) 10-plex reagent, mixed, and fractionated on stage tips packed with strong cation exchange disks. Resulting 6 fractions were analyzed by nanoflow liquid chromatography tandem mass spectrometry (LC-MS/MS) on Q-Exactive Plus Mass spectrometer (Thermo Fisher) coupled with EASY-nLC 1200 system (Thermo Fisher). Data was analyzed on Spectrum Mill Proteomics Workbench (Agilent Technologies) using Mus Musculus (mouse) database containing 46516 entrees and downloaded from Uniprot.org on 12/28/2017. The output of Spectrum Mill analysis was a protein level summary table using “subgroup specific top” settings whereby quantitative information of shared peptides between the subgroups of each group were used for quantitation of only the top subgroup, and remaining subgroups used ratios of only subgroup specific unique peptides to derive protein quantitation values. Statistical analysis was performed using TMT reporter ion ratios of each channel to the median of all channels for all the proteins identified with 2 or more peptides. Ratios were median normalized aligning the data from the IgG samples separately from the Baf47 samples since the amount of proteins pulled down by IgG

was much less than the Baf47. Linear model analysis was used to compare isogenic wildtype versus mutant samples as described previously (40).

Human patient data.

TCGA, PanCancer Atlas patient data were obtained from cBioPortal (41, 42). For transcriptomic analysis of wildtype versus mutant patients, differential expression analysis based on normalized mRNA expression, RSEM (Batch normalized from Illumina HiSeq_RNASeqV2) was retrieved from cBioPortal. For LUAD patients, all up- and downregulated with q-values adjusted by the Benjamani-Hochberg procedure less than 0.05 were classified as differentially expressed. Identical q-value cut offs were used for downstream analysis of endometrial and stomach carcinoma datasets. Gene ontology and cancer pathways analysis using differentially expressed genes was performed using the Panther database (43, 44). Genes with p-value < 0.05, FDR < 0.05 cutoffs were selected, and gene enrichment ratios were calculated. Gene ratio ("Enrichment ratio") based on total genes represented in each pathway was used to generate dot plots. Correlation analysis was performed on lung TCGA data, using the lung cancer explorer portal (45) (http://lce.biohpc.swmed.edu/lungcancer/index.php). For siRNA knockdown studies in Project DRIVE, ATR RSA scores for topmost and bottommost 50 cancer cell lines were tabulated. Cell line genotypes were obtained from published studies using DEPMAP (https://depmap.org/portal/). Similar analysis was performed for CRISPR loss-of-function screens in cancer cell lines from Project Achilles CRISPR Avana 20Q1 datasets downloaded from DEPMAP. ATR and BRG1 gene essentiality were assessed in all lung (n=102) and uterine (n=22) cancer cell lines). Cell lines with BRG1 CERES scores less than −0.70 were filtered to account for cell lines where BRG1 might be essential.

Data availability.

The RNA-sequencing data related to isogenic murine Brg1 wildtype and knockout cells have been deposited in the National Center for Biotechnology Information's Gene Expression Omnibus (GEO) and is accessible through GEO series accession number GSE154266 (https://www.ncbi.nlm.nih.gov/geo/query/acc.cgi?acc=GSE154266). The original Baf47 mass spectrometry data in murine isogenic Brg1 wildtype and knockout cells along with the protein sequence databases used for searches have been deposited in the public proteomics repository MassIVE (https://massive.ucsd.edu) and is accessible through MassIVE accession number MSV000085701 (ftp://massive.ucsd.edu/MSV000085701/).

Statistics and reproducibility.

GraphPad PRISM 8, R software, and Tableau was used for statistical and visual analyses. Sample size and error bars are reported in the figure legends. Exact p-values are shown where possible. Unless otherwise noted, statistical tests were performed using unpaired two-tailed Student's *t*-test. The number of times experiments were performed with similar results is indicated in each legend. p-values less than 0.05 were considered significant.

Results

To identify possible BRG1-dependent functions in lung cancer, we analyzed transcriptomic profiles in LUAD patients from the TCGA, PanCancer cohorts (46, 47). Upregulated genes in *BRG1*-mutant LUAD predominantly belonged to gene ontology (GO) categories associated with DNA replication, elongation, and chromatin remodeling at the centromere (Fig 1a, Supplementary Table 1). Analysis of top upregulated cancer reactome pathways revealed the presence of gene signatures connected to pre-replication and activation of the ATR pathway in response to replication stress (Fig. 1b, Supplementary Fig. S1a, Supplementary Table 1). To rule out effects due to background mutations in patient samples, we utilized the $Kras^{G12D/+}$; $Tp53^{fl/fl}$ (p53) (KP) murine model of LUAD. This model has been shown to recapitulate key features of KRAS-driven human LUAD in several studies (48, 49). We used CRISPR–Cas9-mediated genome-editing with sgRNAs targeting either *Brg1* or *tdTomato* to develop isogenic KP-derived LUAD cell lines (KPB) that led to loss of Brg1 protein (Fig. 1c; n = 2 lines per genotype). RNA-sequencing in isogenic *Brg1* wildtype and knockout cells showed enrichment of DNA replication and replication initiation related GO categories (Supplementary Fig. S1b, Supplementary Table 2). Strikingly, the pathways of pre-replication and ATR activation identified in *BRG1*-mutant patient samples were also among the top upregulated pathways in an isogenic setting of Brg1 loss (Fig. 1d, Supplementary Table 2). We evaluated the two pathways for overlapping genes that are significantly upregulated in both human and murine LUAD and discovered a set of genes strongly linked to early DNA replication and origin firing (that is, CDC6, CDC7, ORC1, among others) (Supplementary Fig. S1c). Expression levels of these genes in the TCGA LUAD data positively correlated with each other and negatively with *BRG1* expression (Supplementary Fig. S1d). To assess whether a replication stress related gene signature would inform future clinical relevance, we combined genes identified in the ATR-related pathway from figures 1b,d with a comprehensive list of genes discovered to be critical for this process (50) (Supplementary Table 3). We found that high expression of replication stress related genes correlated with worse survival in patients with LUAD but not lung squamous cell carcinoma (LSCC) (Supplementary Fig. S1e). These results suggested that BRG1 loss leads to clinically relevant gene expression changes related to replication stress and pre-replication functions.

The presence of increased ATR-related replication stress gene signatures in human and murine LUAD prompted us to measure whether components of the ATR pathway were altered upon BRG1 loss. To study the effects of BRG1 loss in human lung cancers, we engineered isogenic BRG1 wildtype (WT) and knockout (KO) cell lines using CRISPR-Cas9 genome-editing in various NSCLC backgrounds (H460, H2009, and Calu6, n = 3 lines per genotype; Fig. 1e). Reintroduction of BRG1 in BRG1-deficient isogenic cell lines rescued expression of BRG1 (Fig. 1e). Expression levels of core components of the mammalian SWI/SNF complexes including BAF155 and BAF170 were unchanged upon genome-editing of *BRG1* (Supplementary Fig. S1f). ARID1A levels were undetectable in H460 (frameshift mutation), while H2009 and Calu6 showed little to no change between isogenic cell lines. The paralog of BRG1, BRM, is present in SWI/SNF complexes in a mutually exclusive manner and has been documented to compensate for BRG1 loss (51).

BRM protein levels had minimal or no change in H460 and H2009 isogenic cells, whereas Calu6 knockout cells had reduced levels (Supplementary Fig. S1f). BRM gene expression levels were reduced in *BRG1*-mutant LUAD patients compared to that of *BRG1*-wildtype patients (Supplementary Fig. S1g). In order to rule out effects due to changes in LKB1 and KEAP1, we confirmed unchanged levels of these proteins in all isogenic models of BRG1 loss (Supplementary Fig. S1h,i). The integrity of the replication fork is protected in part by an ATR-CHK1-dependent signaling cascade, which is essential for fork stabilization and cell viability (52, 53). We found that loss of BRG1 leads to upregulation of ATR and the activation of the ATR pathway, as measured by phospho-CHK1(Ser345) levels (Fig 1f). In BRG1-rescued isogenic cells, phospho-CHK1 levels were reduced in a BRG1-dependent fashion (Fig. 1f). These data support the hypothesis that loss of BRG1 promotes replication stress related changes leading to activation of ATR-mediated responses.

We next sought to understand how BRG1-deficient cells trigger a replication stress response using single-molecule DNA fiber spreading to assess fork dynamics (39, 54, 55). It is well established that deregulated fork speed is linked to replicative stress in cells (56). Ongoing forks were identified by red-green tracks (Fig. 2a). While BRG1 deficiency did not confer proliferative advantages in lung cancer cells (Supplementary Fig. S2a,b), there was a significant reduction in fork speed in BRG1-deficient cells compared to isogenic controls (approx. 1.5-fold, Fig. 2b,c). Reconstitution with full length BRG1 increased fork speeds; BRG1 KO rescue cells (+BRG1) exhibited a significant increase in fork speeds compared to control BRG1 KO cells (+EMP) (Fig. 2d,e). To explore cell cycle changes upon BRG1 loss, we analyzed asynchronously cycling isogenic cell lines. As with proliferation indices, there was no significant impact of BRG1 loss on cell cycle phases across all our models (Supplementary Fig. S2c,d). For some isogenic pairs, BRG1-deficient lines had more cells in S-phase, which prompted us to examine S-phase lengths (Supplementary Fig. S2c,d). EdU pulse-chase experiments (57) showed delays in the completion of S-phases in BRG1-deficient cells (Supplementary Fig. S2e). Consistent with this, the expression of G1/S and S-phase related cyclin/CDK genes was increased in *BRG1*-mutant LUAD patients. (Supplementary Fig. S2f). To measure whether BRG1-deficient cells harbor efforts to overcome this increase in replication stress, we used quantitative RT-PCR to analyze gene expression for genes associated with replication fork reversal (that is, BLM, WRN, BRCA1, BRAC2, RAD51) and found overall increased gene expression patterns (Supplementary Fig. S2g). These data suggest that lung cancer cells with BRG1 loss have replication fork defects, leading to problems in the proper completion of DNA replication.

Next, we tested if replication stress resulting from BRG1 deficiency undermines genome integrity. We analyzed gamma-H2AX staining patterns to represent less damaged (< 5 foci/cell), more damaged DNA (>5 foci/cell), and replication stress-associated levels (pan-nuclear expression/cell). Detection of gamma-H2AX by immunofluorescence showed a significant increase in the percentage of cells harboring pan-nuclear and high number of gamma-H2AX foci after BRG1 knockout compared to isogenic controls (Fig. 2f,g). Alkaline single-cell comet analysis further confirmed that loss of BRG1 is sufficient to induce DNA damage (Fig. 2h,i). Increased DNA damage is consistent with the observations that *BRG1*-mutant lung cancers have higher mutational burdens compared to other common onco- and tumor suppressors in the lung (46, 47; 58, 59). RPA complexes are linked to the stabilization

of single-strand DNA (ssDNA) intermediates to allow for efficient replication and ATR activation (52, 53). RPA foci were assessed similarly as described for gamma-H2AX. A higher proportion of cells with pan-nuclear RPA2 and high number of foci were found in BRG1-deficient cells (Fig. 2j,k). This indicated the presence of increased amounts of RPA-bound ssDNA, a canonical substrate for the activation of the ATR pathway, in BRG1-deficient cells. Overall, these experiments demonstrate that replication stress and related chromosomal instabilities are major features of BRG1-deficient lung cancer cells.

Next, to uncover differences in replication dynamics in lung cancers due to BRG1 loss, we evaluated the abundance of ongoing replication intermediates through the visualization of DNA fibers (Fig. 3a). Analysis of fiber structures revealed a 2–3-fold increase in green-red-green tracks representative of bidirectional activation of new origins of replication in BRG1-deficient cells (Fig. 3b–d). Interestingly, there was no change in numbers of stalled forks. (Fig. 3b–d, Supplementary Fig. S3a). At the molecular level, replication origins in eukaryotic DNA are identified by the formation of a pre-licensing complex comprised of ORC1–6, CDC6, CDT1, and MCM2–7 proteins. Following pre-licensing complex assembly in G1, origins are activated through S-phase kinases to initiate the duplication of DNA (60, 61). The presence of deregulated origin firing has been previously shown to promote fork replication defects and increase chromosomal breakage (62). Restoring BRG1 levels, however, was sufficient to reduce the presence of new origins of replication to control levels (Fig. 3e–g). Both RNA (Supplementary Fig. S3b,c) and protein (Fig. 3h,i) levels of essential pre-licensing proteins, including CDC6, were upregulated in BRG1-deficient cells and in human *BRG1*-mutant LUAD patients. High CDC6 expression also correlated with poor survival in LUAD patients (Supplementary Fig. S3d). ORC1 was heterogeneously expressed in human isogenic models (Fig. 3h,i). *BRG1* expression negatively correlated with pre-replication related gene expression (Supplementary Fig. S3e). Rescue of BRG1 in BRG1-deficient cells lowered overall levels of CDC6 suggesting specific transcriptomic regulation between *BRG1* and origin firing (Fig. 3h,i). Analysis of patient-derived xenograft (PDX) cell lines recapitulated pre-replication defects observed in the human isogenic models (Supplementary Fig. S3f). These data suggest that the replication stress related to the loss of BRG1 in lung cancers could be a consequence of excessive and uncontrolled origin firing and fork response mechanisms, albeit at the cost of increasing amounts of chromosomal instability.

Since BRG1-deficiency causes replication stress, we hypothesized that BRG1-containing SWI/SNF complexes may be engaged in protein interactions at forks to allow for efficient replication progression. To explore the proteome associated with SWI/SNF complexes in a defined system, we turned to our isogenic murine models. We performed co-immunoprecipitations in KP and KPB cells, using a core component of the complex, Baf47/Smarcb1, as bait. Baf47 is part of two major classes of mammalian SWI/SNF complexes, canonical BAF (cBAF) and polybromo-associated BAF (PBAF), while the recently characterized non-canonical BAF (ncBAF) complexes were shown to lack Baf47 incorporation (3–8). We quantified the abundance of Baf47 protein interactors using quantitative mass spectrometry (Fig. 4a and Supplemental Table 4). Quantification of SWI/SNF subunit compositions showed that residual complexes in Brg1-deficient cells were enriched for subunits Brm, Ss18l1, Dpf2, and Smarcd1. Mammalian SWI/SNF ATPase-

dependent subunits including Ss18, Pbrm1, Actl6a, Bcl7 were identified predominantly in Brg1 wildtype cells, as also shown by others (63) (Supplementary Fig. S4a). Enrichment of Baf47 between KP and KPB cells was approximately equal with an overall fold change of −0.065 (Fig. 4b). Compared to proteins enriched at the fork (64), proteins enriched in Brg1 wildtype cells were associated with the GO category pre-replicative complex assembly (Fig. 4c). In Brg1-deficient cells, the top GO categories were associated with ssDNA repair and DNA damage response, consistent with our findings of increased RPA2 foci and presence of replication stress in human isogenic BRG1-deficient cells (Fig. 4c). The detection of known and expected interactions with Baf47 motivated us to look further into tumor-specific interactions dependent on Brg1 expression in lung cancer cells, particularly those that functioned in the context of replication stress. Interestingly, Rpa1, the largest protein of the heterotrimeric RPA complex, and MCM-related proteins (Mcm6, Mcm7) were strongly depleted in the Brg1-deficient setting (Fig. 4b, Supplementary Fig. S4a). Since the RPA heterotrimer is critical for the protection of ssDNA during physiological DNA processes such as replication, repair, and has been shown to be involved in replication initiation and elongation (65, 66), we hypothesized that BRG1 might associate with the RPA complex during DNA replication.

We next used co-immunoprecipitation (co-IP) to test the idea that BRG1-containing SWI/SNF complexes associate with RPA complexes for fork progression and to prevent DNA breakage. Consistent with our hypothesis, we observed that RPA1 and RPA2 immunoprecipitated with BRG1 in human BRG1 wildtype cells (Fig. 4d, Supplementary Fig. S4b). In isogenic models of BRG1 loss, the interaction between the SWI/SNF complexes and RPA complex was lost (Fig. 4d). This suggested that the interaction between the two complexes is dependent on BRG1. Furthermore, BRG1 reconstitution restored these interactions, confirming they depend on intact BRG1 (Supplementary Fig. S4c). Interactions between BRG1-containing SWI/SNF complexes and RPA were also confirmed with antibodies against BAF47 and BAF170 in isogenic BRG1 contexts (Fig. 4e,f, Supplementary Fig. S4d,e). Co-IP also showed evidence for interactions between residual SWI/SNF complexes and ORC1, important for selecting replication origin sites (Supplementary Fig. S4f). These interactions were however found to be independent of BRG1. We were unable to detect any interactions between BRG1 and TOPBP1 (21) (Supplementary Fig. S4g). Taken together, these findings suggest that BRG1-containing SWI/SNF complexes associate with ssDNA-bound RPA complexes and origin recognition protein ORC1, and loss of these interactions upon BRG1 loss could lead to defective fork progression.

Lastly, we investigated whether the increased reliance on the ATR pathway in BRG1-deficient lung cancers could be exploited as a therapeutic vulnerability. We screened a set of small molecule compounds targeted towards proteins involved in regulating aspects of DNA damage response and repair (Supplementary Fig. S5a). Isogenic BRG1-deficient cells were only sensitive to the treatment with either an ATR inhibitor (VX-970/M6620 (67)) or an inhibitor targeting its downstream effector kinase CHK1 (MK-8776 (68, 69)). The indistinguishable responses in viability between isogenic BRG1 proficient and deficient cells to ATM or PARP inhibition suggested that the DNA repair responses were largely unaffected despite the absence of BRG1 in lung cancer cells (Supplementary Fig. S5a,b). Responses to aurora kinase A inhibitor VX-680 (70) and CDK4/6 (71) inhibitor palbociclib were also

identical between BRG1 proficient and deficient cells (Supplementary Fig. S5a,c). These experiments suggest that inhibition of the ATR pathway suppresses tumor growth in *BRG1*-deficient lung cancers by targeting the replication stress response.

We used several experimental systems to explore the ATR-inhibitor sensitivity of BRG1-deficient lung cancer cells. Human BRG1-deficient cells showed a robust 3–6-fold higher sensitization to ATR inhibition compared to isogenic BRG1 wildtype cells, and reconstitution with BRG1 was able to restore this sensitivity back to control levels (Fig. 5a). Using a panel of human NSCLC cell lines, reduced values of VX-970 IC50s were observed in *BRG1*-mutant NSCLC cell lines which predicted sensitivity to ATR inhibition (Supplementary Fig. S5d). Murine isogenic KPB cells were 3–5-fold more sensitive to ATR inhibition (Fig. 5b). Further *in vitro* validation with cell lines derived from KRAS mutant LUAD PDX models showed that *BRG1* mutations was sufficient for a 7-fold reduction in cell viability upon treatment with ATR inhibitors (Fig. 5c). To determine if additional replication stress could further enhance responses to ATR inhibition, we combined ATR inhibition with topoisomerase I inhibitor irinotecan to induce ssDNA breaks or hydroxyurea to cause deoxyribonucleotide depletion. Combinatorial treatment experiments further suppressed growth at nanomolar range concentrations of ATR inhibitors (Supplementary Fig. S5e,f). These findings demonstrate that loss of BRG1 creates a targetable dependence on the ATR pathway and the replication stress response in lung cancers.

We hypothesized that the replication dynamics in BRG1-deficient cells could be altered by the inhibition of ATR, given its role in replication stress responses. ATR inhibition further increased origin firing in BRG1-deficient cells and led to accumulation of stalled forks, as indicated through the presence single red track fibers (Fig. 5d,e). Single-molecule comet analysis of human isogenic cells treated with ATR inhibition revealed increased DNA breaks only in BRG1-deficient cells (Supplementary Fig. S5g–i). This suggests that ATR activation serves as an important molecular barrier to prevent further genomic instability to allow BRG1-deficient cancer cells to survive.

To investigate the therapeutic efficacy of targeting BRG1-deficient lung cancer cells with ATR inhibition in vivo, we transplanted human isogenic BRG1 wildtype and knockout cells subcutaneously into immunodeficient mice. Following the establishment of tumors, we initiated treatment with either vehicle or VX-970. While BRG1 wildtype tumors exhibited no changes in tumor growth dynamics, BRG1-deficent tumors showed robust reductions in overall tumor size after treatment with ATR inhibition (Fig. 5f, Supplementary Fig. S5j).

Thus, *in vitro* and *in vivo* susceptibility of BRG1-deficient lung cancers to ATR inhibitors provides a possible therapeutic path based on defects in replication.

Finally, we wondered if other cancers with *BRG1* mutations behave similarly to lung cancers. Data from cancer datasets showed that mutation of *BRG1* is also linked to other carcinoma types including endometrial (15%), stomach (8%), and rare ovarian cancers (72) (100%) (Supplementary Fig. S6a,b). Gene expression and pathway analysis confirmed a conserved replication stress response in other cancer types with *BRG1* mutations (Supplementary Fig. S6c–e). An upregulated gene signature of 66 genes derived from lung,

endometrial, and stomach adenocarcinoma patients predicted poor prognosis in patients with LUAD (Supplementary Fig. S6f,g). Furthermore, analysis of synthetic lethality RNAi screening data from Project DRIVE (73) uncovered a high correlation between sensitivity to ATR knockdown and mutations in SWI/SNF ATPases BRG1/BRM across cancer cell lines representing different tissue types (Fig. 6a,b). While *BRG1* was the predominant SWI/SNF ATPase mutated in all lines, *BRM* alone was mutated in only 4/50 of most sensitive cell lines (Supplementary Table 5). Cancer cell lines with different kinds of *BRG1/BRM* mutations were found to be vulnerable to ATR knockdown (Fig. 6c). Interestingly, cell lines that had missense mutations – NCIH-1435 (lung), NCIH-2126 (lung), NCIH-23 (lung) are among the most sensitive to ATR knockdown (Supplementary Table 5). These findings provide novel insight into the synthetic lethal relationship between BRG1 and ATR in lung as well as other cancer types with mutations in *BRG1*.

We corroborated these findings in CRISPR knockout screens using dependency data from Project ACHILLES (74, 75). We assessed ATR and BRG1 gene essentiality scores (CERES) in lung and uterine cancer cell lines. Among lung cancer lines with ATR CERES scores less than median gene essential score of −1, 40% of lung cell lines had mutations in *BRG1/BRM*, and 63% in uterine cancer lines (Fig. 6d–i, Supplementary Table 5). ATR was essential in cell lines bearing both missense and truncating mutations. These findings further support the conclusion that mutations in *BRG1* can predict ATR dependency.

Discussion

This study provides novel insight for the role of *BRG1* and mammalian SWI/SNF complexes in lung cancer progression. We found that BRG1 plays an important role in preventing replication stress and that BRG1 may regulate origin firing in lung cancers. Our data suggest that BRG1-containing SWI/SNF complexes interact with ssDNA-binding protein RPA; thus, BRG1 may impact the function of RPA at replication forks. Our data further suggest a link between SWI/SNF complex and ORC1, suggesting a potential role for BRG1 in licensing or firing of origins. Knockout of BRG1 in lung cancer isogenic models led to slowing of replication, induction of replication stress, increased origin firing, and activation of the ATR checkpoint pathway. The replication defects and the ATR dependence we observed provide a possible explanation for how lung cancer cells tolerate BRG1 loss and survive in the presence of genome instability.

Our studies revealed novel potential protein interactions of SWI/SNF complexes that depend on BRG1 in lung cancers. It is important to note that loss or mutation of BRG1 in lung cancers may alter compositions of residual SWI/SNF complexes, such as cBAF, PBAF, and ncBAF; our study did not address this question. Further interrogation of how subcomplex identity affects replication stress responses will be important in future studies. We observed RPA complex interactions by co-IP with complex subunits BRG1, BAF47, and BAF170 in BRG1 wildtype lung cancer cells. The RPA heterotrimer is linked to the protection of ssDNA during replication and also serves to recruit ATR/ATRIP during events of replication stress (52, 53). We speculate that loss of BRG1 disrupts the binding of SWI/SNF and RPA, thereby allowing RPA to bind ssDNA at replication forks more efficiently. We suggest that this interaction leads to activation of ATR at stressed replication forks, creating a

dependency on ATR to protect such forks. It is also likely that loss of BRG1 promotes changes at the nucleosome accessibility level, which could in turn affect the replisome landscape (76). Thus, reduced interactions between SWI/SNF and RPA complexes and increased chromatin compaction could contribute to replicative stress and ATR dependence in BRG1-deficient lung cancer cells.

We hypothesize that loss of BRG1 function leads to reduced fork speeds in lung cancer cells, providing an opportunity for increased origin firing to compensate for fork defects. We uncovered increased origin firing and increased CDC6 levels in BRG1-deficient lung cancer cells, consistent with this hypothesis. Firing of ongoing and dormant origins of replication is often an important compensatory mechanism to prevent fork stress-related defects from causing damage in cells (77, 78). The slowing or stalling of replication forks provides an opportunity for dormant origins to fire, which could also be assisted by the increased levels of CDC6 in BRG1-deficient cells. Elevation of origin firing in BRG1-deficient cells could also increase the number of replication forks slowed or stalled by compacted chromatin, increasing the consumption of dNTPs in cells and further promoting replication stress and genomic instability. This model could explain why BRG1 loss leads to a significant increase of replication stress and genomic instability in lung cancer. Thus, our data suggests that rather than simply promoting increased proliferation rates, mutations in *BRG1* may serve as a driving mechanism for advancing tumorigenesis by increasing genomic instability visa vie replicative stress.

Mutations in *BRG1* account for at least 10% of all NSCLC, with no currently approved precision medicine available for these patients. Clinicopathologic features of lung cancers have linked BRG1-deficiency with primary resistance to standard treatments (14). Our results suggest that ATR activity is a critical barrier to prevent eventual mitotic catastrophe in *BRG1*-mutant lung cancers, revealing a new potential vulnerability for therapeutic targeting. Our findings show that loss of BRG1 might be an important biomarker in lung cancer patients that could benefit from ATR inhibition therapy. Interestingly, deletion of *ARID1A*, another member of the SWI/SNF complex, in colon cancer cells has been connected to sensitivity to ATR inhibitors (79). Of note, the lung cancer cell line H460 used in this study has an *ARID1A* mutation with undetectable levels of ARID1A protein. Deletion of BRG1 in this ARID1A mutant lung cancer background increased sensitivity to ATR inhibitors. Our data in lung cancer cells, combined with our analysis of ATR dependency screens in multiple cancer types, suggests that targeting ATR may represent a broad therapeutic strategy for patients with mutations in subunits of SWI/SNF complexes. ATR inhibitors are currently being tested in the clinic for other cancers (80). We suggest that it will be particularly fruitful to test ATR inhibition as therapy for patients with *BRG1*-mutant lung cancers and other BRG1-deficient cancers that exhibit replication stress responses.

Supplementary Material

Refer to Web version on PubMed Central for supplementary material.

Acknowledgements

We would like to thank members of the Kim Lab, Raul Mostoslavsky, Cigall Kadoch, Peter Sicinski, and Lynette Scholl for helpful discussions. M.G. has been supported by the Albert J. Ryan graduate fellowship. C.P.C is supported by the American Cancer Society (ACS) postdoctoral fellowship 130361-PF-17-009-01-CDD and the Koch Institute (KI) Quinquennial Postdoctoral Fellowship. C.F.B is supported by grants from the National Institute of General Medical Sciences (NIGMS) P20-GM121327-03, National Cancer Institute (NCI) R01-CA237643, and the ACS Research Scholar Grant 133123-RSG-19-081-01-TBG. Mass spectrometry/analysis was performed at the Broad Institute and was supported in part by grants from the NCI Clinical Proteomic Tumor Analysis Consortium grants NIH/NCI U24-CA210986 and NIH/NCI U01-CA214125 (to SAC) and NIH/NCI U24-CA210979 (to DRM). K.K.W was funded by NCI R01-CA216188, R01-CA205150 and U01-CA213333. T.J is supported by grants from Howard Hughes Medical Institute, Ludwig Center for Molecular Oncology at MIT, NIH P01 Jacks P01-CA42063, The Bridge Project, a partnership between the Koch Institute for Integrative Cancer Research at MIT and the Dana-Farber/Harvard Cancer Center (DF/HCC), and grants from the NCI KI Cancer Center Support Grant P30-CA14051. C.F.K is supported by NIH/NCI R01-CA216188, ACS Mission Boost Grant 71647, and DF/HCC Bridge Grant 72387.

References

1. Stewart BW, & Wild CP (n.d.). World cancer report 2014.
2. Cardarella S & Johnson BE The impact of genomic changes on treatment of lung cancer. Am. J. Respir. Crit. Care Med 188, 770–775 (2013). [PubMed: 23841470]
3. Kadoch Cigall, and Crabtree Gerald R. “Mammalian SWI/SNF chromatin remodeling complexes and cancer: Mechanistic insights gained from human genomics.” Science advances vol. 1,5 e1500447 (2015) [PubMed: 26601204]
4. Wilson Boris G, and Roberts Charles W M. “SWI/SNF nucleosome remodellers and cancer.” Nature reviews. Cancer vol. 11,7 481–92. 9 (2011) [PubMed: 21654818]
5. Michel Brittany C et al. “A non-canonical SWI/SNF complex is a synthetic lethal target in cancers driven by BAF complex perturbation.” Nature cell biology vol. 20,12 141–20 (2018)
6. Alpsoy A, Dykhuizen EC. Glioma tumor suppressor candidate region gene 1 (GLTSCR1) and its paralog GLTSCR1-like form SWI/SNF chromatin remodeling subcomplexes. J Biol Chem. 293 (11):3892–3903. (2018) [PubMed: 29374058]
7. Gatchalian J, Malik S, Ho J, et al. A non-canonical BRD9-containing BAF chromatin remodeling complex regulates naive pluripotency in mouse embryonic stem cells. Nat Commun. 9 (1):5139 (2018) [PubMed: 30510198]
8. Wang X, Wang S, Troisi EC, et al. BRD9 defines a SWI/SNF sub-complex and constitutes a specific vulnerability in malignant rhabdoid tumors. Nat Commun. 10 (1):1881 (2019) [PubMed: 31015438]
9. Wong AKC et al. BRG1, a component of the SWI-SNF complex, is mutated in multiple human tumor cell lines. Cancer Res. 60, 6171–6177 (2000). [PubMed: 11085541]
10. Reisman DN, Sciarrotta J, Wang W, Funkhouser WK & Weissman BE Loss of BRG1/BRM in Human Lung Cancer Cell Lines and Primary Lung Cancers: Correlation with Poor Prognosis 1. Cancer Res. 63, (2003).
11. Medina PP et al. Frequent BRG1/SMARCA4-Inactivating mutations in human lung cancer cell lines. Hum. Mutat 29, 617–622 (2008). [PubMed: 18386774]
12. Rodriguez-Nieto S et al. Massive parallel DNA pyrosequencing analysis of the tumor suppressor BRG1/SMARCA4 in lung primary tumors. Hum. Mutat 32, (2011).
13. Rodriguez-Nieto S & Sanchez-Cespedes M BRG1 and LKB1: Tales of two tumor suppressor genes on chromosome 19p and lung cancer. Carcinogenesis 30, 547–554 (2009). [PubMed: 19176640]
14. Dagogo-Jack Ibiayi et al. Clinicopathologic Characteristics of BRG1-Deficient NSCLC. Journal of thoracic oncology 20, S1556–0864 (2020)
15. Bultman S et al. A Brg1 Null Mutation in the Mouse Reveals Functional Differences among Mammalian SWI/SNF Complexes. Mol. Cell 6, 1287–1295 (2000). [PubMed: 11163203]
16. Glaros S, Cirrincione GM, Palanca A, Metzger D & Reisman D Targeted knockout of BRG1 potentiates lung cancer development. Cancer Res. 68, 3689–3696 (2008). [PubMed: 18483251]

17. Marquez-Vilendrer SB, Rai SK, Gramling SJ, Lu L & Reisman DN Loss of the SWI/SNF ATPase subunits BRM and BRG1 drives lung cancer development. Oncoscience 3, 322–336 (2016). [PubMed: 28105457]
18. Chung W-JJ et al. Kras mutant genetically engineered mouse models of human cancers are genomically heterogeneous. Proc. Natl. Acad. Sci. U. S. A 114, E10947–E10955 (2017). [PubMed: 29203670]
19. Dykhuizen EC et al. BAF complexes facilitate decatenation of DNA by topoisomerase IIα. Nature 497, 624–627 (2013). [PubMed: 23698369]
20. Bourgo RJ et al. SWI/SNF deficiency results in aberrant chromatin organization, mitotic failure, and diminished proliferative capacity. Mol. Biol. Cell 20, 3192–3199 (2009). [PubMed: 19458193]
21. Cohen SM et al. BRG1 co-localizes with DNA replication factors and is required for efficient replication fork progression. Nucleic Acids Res. 38, 6906–6919 (2010). [PubMed: 20571081]
22. Dunaief JL et al. The retinoblastoma protein and BRG1 form a complex and cooperate to induce cell cycle arrest. Cell 79, 119–130 (1994). [PubMed: 7923370]
23. Dimitrova Nadya et al. “Stromal Expression of miR-143/145 Promotes Neoangiogenesis in Lung Cancer Development.” Cancer discovery vol. 6,2 (2016)
24. Ran FA et al. Genome engineering using the CRISPR-Cas9 system. Nature protocols 8, 2281–2308, doi:10.1038/nprot.2013.143 (2013). [PubMed: 24157548]
25. Sánchez-Rivera FJ et al. Rapid modelling of cooperating genetic events in cancer through somatic genome editing. Nature 516, 428–431, doi:10.1038/nature13906 (2014). [PubMed: 25337879]
26. Shalem O et al. Genome-Scale CRISPR-Cas9 Knockout Screening in Human Cells. Science 343, 84–87, doi:10.1126/science.1247005 (2014). [PubMed: 24336571]
27. Fillmore CM et al. Estrogen expands breast cancer stem-like cells through paracrine FGF/Tbx3 signaling. Proceedings of the National Academy of Sciences 107, 21737–21742 (2010).
28. Xi Q, He W, Zhang XH-F, Le H-V & Massagué J Genome-wide impact of the BRG1 SWI/SNF chromatin remodeler on the transforming growth factor beta transcriptional program. J. Biol. Chem 283, 1146–1155 (2008). [PubMed: 18003620]
29. Zacharek SJ et al. Lung stem cell self-renewal relies on bmi1-dependent control of expression at imprinted loci. Cell Stem Cell 9, 272–281 (2010).
30. Fillmore CM et al. EZH2 inhibition sensitizes BRG1 and EGFR mutant lung tumours to TopoII inhibitors. Nature 520, 239–242 (2015). [PubMed: 25629630]
31. Li Bo, and Dewey Colin N. “RSEM: accurate transcript quantification from RNA-Seq data with or without a reference genome.” BMC bioinformatics vol. 12 323 (2011) [PubMed: 21816040]
32. Langmead Ben et al. “Ultrafast and memory-efficient alignment of short DNA sequences to the human genome.” Genome biology vol. 10,3 (2009)
33. Leng Ning et al. “EBSeq: an empirical Bayes hierarchical model for inference in RNA-seq experiments.” Bioinformatics (Oxford, England) vol. 29,8 1035–43 (2013)
34. Anders Simon, and Huber Wolfgang. “Differential expression analysis for sequence count data.” Genome biology vol. 11,10 (2010)
35. Bult Carol J et al. “Mouse Genome Database (MGD) 2019.” Nucleic acids research vol. 47,D1 801–806 (2019)
36. Subramanian Aravind et al. “Gene set enrichment analysis: a knowledge-based approach for interpreting genome-wide expression profiles.” Proceedings of the National Academy of Sciences of the United States of America vol. 102,43 15545–50 (2005) [PubMed: 16199517]
37. Liberzon Arthur et al. “The Molecular Signatures Database (MSigDB) hallmark gene set collection.” Cell systems vol. 1,6 417–425 (2015) [PubMed: 26771021]
38. Gyorffy B, Surowiak P, Budczies J, Lanczky A. Online survival analysis software to assess the prognostic value of biomarkers using transcriptomic data in non-small-cell lung cancer, PLoS One, doi: 10.1371/journal.pone.0082241(2013)
39. Nieminuszczy J, Schwab RA & Niedzwiedz W The DNA fibre technique – tracking helicases at work. Methods 108, 92–98 (2016). [PubMed: 27102626]
40. Li J et al. Cell-surface proteomic profiling in the fly brain uncovers wiring regulators. Cell. vol. 180,2 (2020): 373–386.e15. doi:10.1016/j.cell.2019.12.029 (2020) [PubMed: 31955847]

41. Cerami E et al. The cBio cancer genomics portal: an open platform for exploring multidimensional cancer genomics data. Cancer Discov. 2, 401–404 (2012). [PubMed: 22588877]
42. Gao J et al. Integrative analysis of complex cancer genomics and clinical profiles using the cBioPortal. Sci. Signal 6, pl1–pl1 (2013). [PubMed: 23550210]
43. Mi H, Muruganujan A & Thomas PD PANTHER in 2013: modeling the evolution of gene function, and other gene attributes, in the context of phylogenetic trees. Nucleic Acids Res. 41, D377–D386 (2013). [PubMed: 23193289]
44. Thomas PD et al. PANTHER: a library of protein families and subfamilies indexed by function. Genome Res. 13, 2129–2141 (2003). [PubMed: 12952881]
45. Cai L et al. LCE: an open web portal to explore gene expression and clinical associations in lung cancer. Oncogene 38, 2551–2564 (2019). [PubMed: 30532070]
46. Collisson EA et al. Comprehensive molecular profiling of lung adenocarcinoma: The cancer genome atlas research network. Nature 511, 543–550 (2014). [PubMed: 25079552]
47. Hoadley KA et al. Cell-of-Origin Patterns Dominate the Molecular Classification of 10,000 Tumors from 33 Types of Cancer. Cell 173, 291–304.e6 (2018). [PubMed: 29625048]
48. DuPage M, Dooley AL & Jacks T Conditional mouse lung cancer models using adenoviral or lentiviral delivery of Cre recombinase. Nat. Protoc 4, 1064–1072 (2009). [PubMed: 19561589]
49. Jackson EL et al. The differential effects of mutant p53 alleles on advanced murine lung cancer. Cancer Res. 65, 10280–10288 (2005). [PubMed: 16288016]
50. Kavanaugh G et al. A whole genome RNAi screen identifies replication stress response genes. DNA Repair (Amst). 35, 55–62 (2015). [PubMed: 26454783]
51. Papillon JPN et al. Discovery of Orally Active Inhibitors of Brahma Homolog (BRM)/SMARCA2 ATPase Activity for the Treatment of Brahma Related Gene 1 (BRG1)/SMARCA4-Mutant Cancers. J Med Chem. 61(22) : 10155–10172 (2018) [PubMed: 30339381]
52. Gaillard H, García-Muse T & Aguilera A Replication stress and cancer. Nature Reviews Cancer 15, 276–280 (2015). [PubMed: 25907220]
53. Yazinski SA & Zou L Functions, Regulation, and Therapeutic Implications of the ATR Checkpoint Pathway. Annu. Rev. Genet 50, 155–173 (2016). [PubMed: 27617969]
54. Bensimon A et al. Alignment and Sensitive Detection of DNA by a Moving Interface. New Series. 265, (1994).
55. Merrick CJ, Jackson D & Diffley JFX Visualization of Altered Replication Dynamics after DNA Damage in Human Cells. J. Biol. Chem 279, 20067–20075 (2004). [PubMed: 14982920]
56. Maya-Mendoza A et al. High speed of fork progression induces DNA replication stress and genomic instability. Nature 559, 279–284 (2018). [PubMed: 29950726]
57. Pereira PD et al. Quantification of cell cycle kinetics by EdU (5-ethynyl-2'-deoxyuridine)-coupled-fluorescence-intensity analysis. Oncotarget 8, 40514–40532 (2017). [PubMed: 28465489]
58. Imielinski M et al. Mapping the hallmarks of lung adenocarcinoma with massively parallel sequencing. Cell 150, 1107–1120 (2012). [PubMed: 22980975]
59. Zehir A et al. Mutational landscape of metastatic cancer revealed from prospective clinical sequencing of 10,000 patients. Nat. Med 23, 703–713 (2017). [PubMed: 28481359]
60. Bell SP & Dutta A DNA Replication in Eukaryotic Cells. Annu. Rev. Biochem 71, 333–374 (2002). [PubMed: 12045100]
61. Diffley JFX Regulation of early events in chromosome replication. Current Biology 14, (2004).
62. Neelsen KJ et al. Deregulated origin licensing leads to chromosomal breaks by rereplication of a gapped DNA template. Genes Dev. 27, 2537–2542 (2013). [PubMed: 24298053]
63. Pan Joshua et al. The ATPase module of mammalian SWI/SNF family complexes mediates subcomplex identity and catalytic activity-independent genomic targeting. Nature genetics vol. 51, 4 618–626 (2019) [PubMed: 30858614]
64. Wessel SR, Mohni KN, Luzwick JW, Dungrawala H & Cortez D Functional Analysis of the Replication Fork Proteome Identifies BET Proteins as PCNA Regulators. Cell Rep. 28, 3497–3509.e4 (2019). [PubMed: 31553917]
65. Fairman M P, and B Stillman. Cellular factors required for multiple stages of SV40 DNA replication in vitro. The EMBO journal vol. 7,4 1211–8 (1988) [PubMed: 2841119]

66. Zou Yue et al. Functions of human replication protein A (RPA): from DNA replication to DNA damage and stress responses. Journal of cellular physiology vol. 208,2 267–73 (2006) [PubMed: 16523492]

67. Knegtel R et al. Rational Design of 5-(4-(Isopropylsulfonyl)phenyl)-3-(3-(4-((methylamino)methyl)phenyl)isoxazol-5-yl)pyrazin-2-amine (VX-970, M6620): Optimization of Intra- and Intermolecular Polar Interactions of a New Ataxia Telangiectasia Mutated and Rad3-Related (ATR. J. Med. Chem 62, 5547–5561 (2019). [PubMed: 31074988]

68. Dwyer MP et al. Discovery of pyrazolo[1,5-a]pyrimidine-based CHK1 inhibitors: A template-based approach—Part 1. Bioorg. Med. Chem. Lett 21, 467–470 (2011). [PubMed: 21094608]

69. Dwyer MP et al. Discovery of pyrazolo[1,5-a]pyrimidine-based CHK1 inhibitors: A template-based approach—Part 2. Bioorg. Med. Chem. Lett 21, 471–474 (2011). [PubMed: 21094607]

70. Tagal V et al. SMARCA4-inactivating mutations increase sensitivity to Aurora kinase A inhibitor VX-680 in non-small cell lung cancers. Nat. Commun 8, 14098 (2017). [PubMed: 28102363]

71. Xue Y et al. SMARCA4 loss is synthetic lethal with CDK4/6 inhibition in non-small cell lung cancer. Nat. Commun 10, 557 (2019). [PubMed: 30718506]

72. Jelinic P et al. Recurrent SMARCA4 mutations in small cell carcinoma of the ovary. Nat. Genet 46, 424–426 (2014). [PubMed: 24658004]

73. McDonald ER et al. Project DRIVE: A Compendium of Cancer Dependencies and Synthetic Lethal Relationships Uncovered by Large-Scale, Deep RNAi Screening. Cell 170, 577–592.e10 (2017). [PubMed: 28753431]

74. Meyers RM et al. Computational correction of copy number effect improves specificity of CRISPR–Cas9 essentiality screens in cancer cells. Nat. Genet 49, 1779–1784 (2017) [PubMed: 29083409]

75. Tsherniak A et al. Defining a cancer dependency map. Cell 170, 564–576 (2017). [PubMed: 28753430]

76. Azmi Ishara F et al. Nucleosomes influence multiple steps during replication initiation. eLife vol. 6 e22512 (2017) [PubMed: 28322723]

77. Brambati Alessandra et al. Dormant origins and fork protection mechanisms rescue sister forks arrested by transcription. Nucleic acids research vol. 46,3 1227–1239 (2018) [PubMed: 29059325]

78. Alver Robert C et al. The contribution of dormant origins to genome stability: from cell biology to human genetics. DNA repair vol. 19,100, 182–9 (2014) [PubMed: 24767947]

79. Williamson Chris T et al. ATR inhibitors as a synthetic lethal therapy for tumours deficient in ARID1A. Nature Communications vol. 7 13837 (2016)

80. Lecona E & Fernandez-Capetillo O Targeting ATR in cancer. Nat. Rev. Cancer 18, 586–595 (2018). [PubMed: 29899559]

Statement of significance

Findings indicate that inhibition of ATR is a promising therapy for the 10% of non-small cell lung cancer patients harboring mutations in SMARCA4/BRG1.

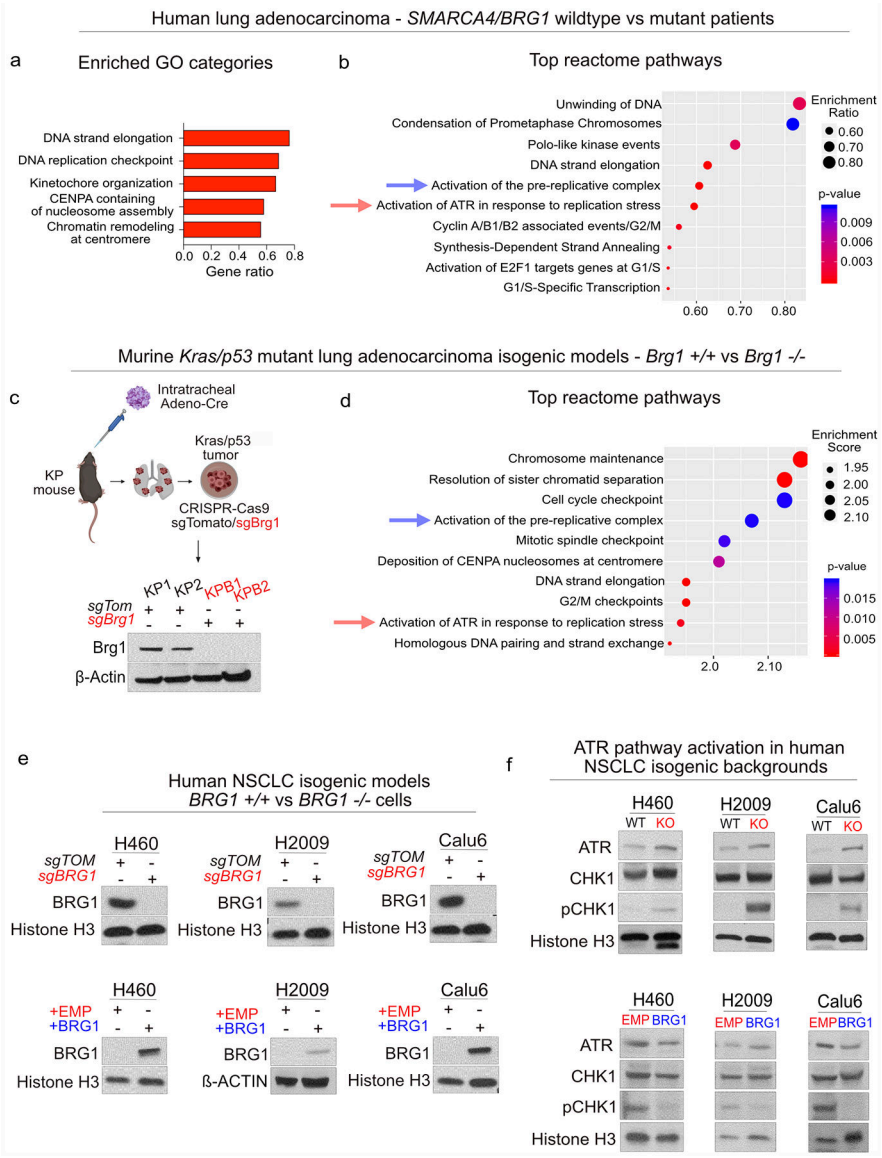

Figure 1. Mutations in BRG1 correlate with increased pre-replication and ATR-related gene signatures in lung cancers.

a, GO analysis of upregulated genes in 51 human *BRG1*-mutant LUAD versus 503 BRG1-wildtype patients.

b, Dot plot of top cancer pathways enriched in *BRG1*-mutant LUAD. Arrows indicate pathways of interest.

c, (top) Schematic of *Brg1* gene-editing in KP mouse LUAD cells. (bottom) Brg1 western blot.

d, Dot plot of top cancer pathways in isogenic murine LUAD Brg1 knockout cells.

e, Western blot in human isogenic models of BRG1 loss.

f, ATR activity western blot in human isogenic models of BRG1 loss.

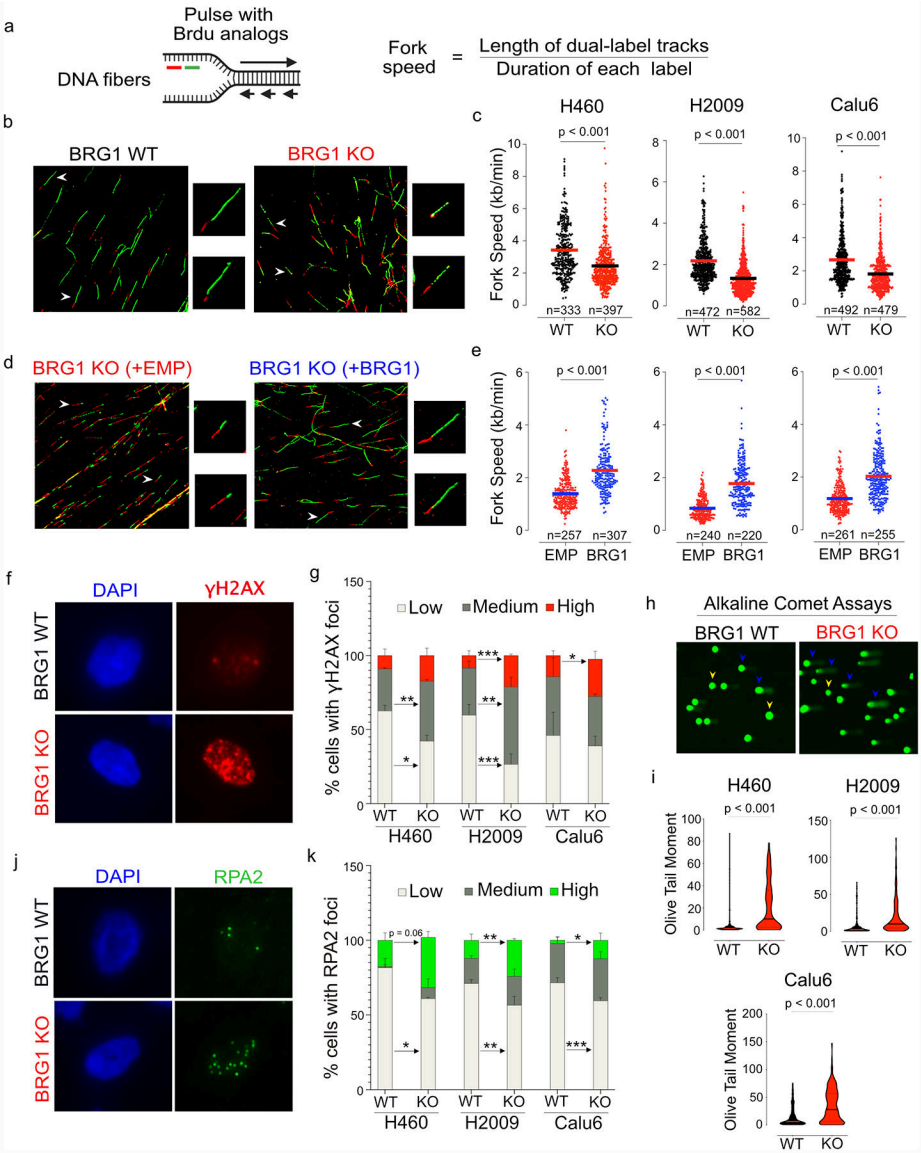

Figure 2. Human isogenic lung cancer cells acquire replication stress and genome instability upon BRG1 deletion.

a, Schematic of DNA fibers labeling strategy.

b-e, Representative ongoing DNA fibers in human isogenic models of BRG1 loss **(b,c)** and overexpression **(d,e)**. Insets show individual fibers (white arrowheads). (n = 2–3 for each cell line).

f,g, Immunofluorescence show representative gamma-γH2AX foci formation and count analysis in human isogenic models of BRG1 loss. (n = 2–3 for each cell line).

h,i, Comet analysis in human isogenic models of BRG1 loss. Yellow arrowheads indicate relatively undamaged nuclei whereas blue arrowheads indicate relatively higher damaged nuclei. (n = 3–4 for each cell line).

j,k, Immunofluorescence show representative RPA2 foci formation and count analysis in human isogenic models of BRG1 loss. (n = 2–3 for each cell line).

All images to scale, and all data is mean ± SD,* $p < 0.05$, ** $p < 0.01$, *** $p < 0.005$, **** $p < 0.001$.

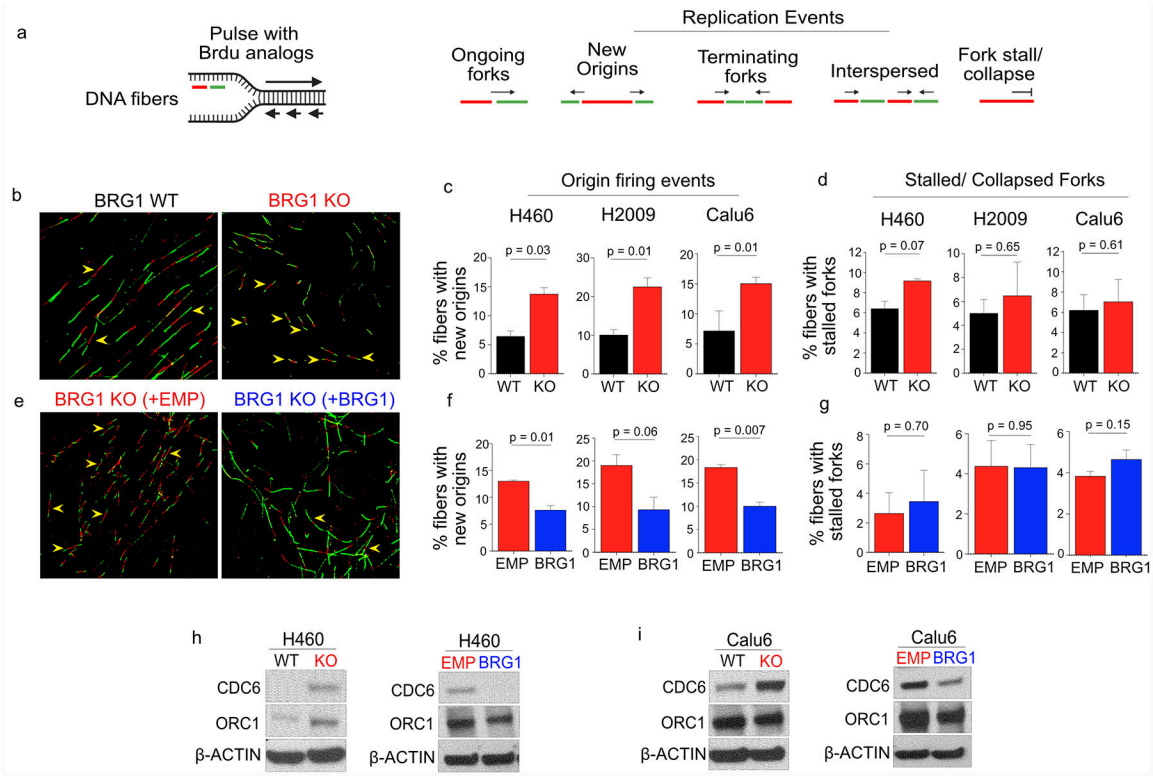

Figure 3. Analysis of ongoing DNA fibers implicate defects in pre-replication upon loss of SWI/SNF complex activity.

a, Schematic of predicted replication events using DNA fibers.

b-g, Representative DNA fiber spreads and analysis of origin firing/stalled forks in human isogenic models of BRG1 loss **(b-f)** and overexpression **(e-g)**. Green-red-green tracks indicative of new origins of replication are shown with yellow arrowheads. All data is mean ± SD. (n = 2–3 for each cell line).

h,i, Western blot for pre-replication proteins in human isogenic models of BRG1 loss and overexpression.

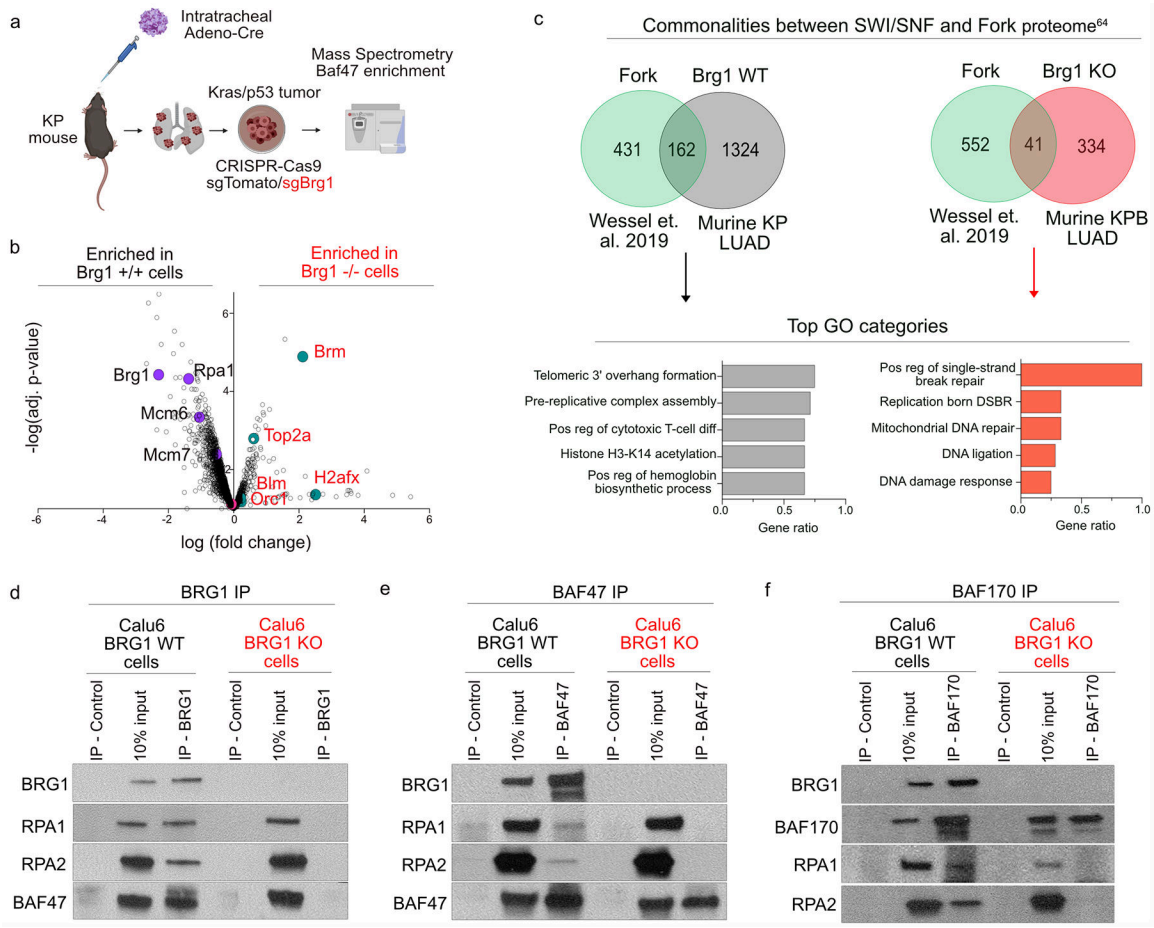

Figure 4. Biochemical analysis of the mammalian SWI/SNF complex couples BRG1 with ongoing DNA replication via the RPA complex.

a, Schematic of Baf47 co-IP performed in murine isogenic models of Brg1 loss.

b, Volcano plot depicting whole proteome enrichment. Candidate proteins in each genotype are color-coded (wildtype – grape, knockout – teal) based on fold change (x-axis) and p-value (y-axis). Baf47 was equally enriched in wildtype and knockout cells (pink dot).

c, GO categories for proteins commonly identified between *Brg1* wildtype or knockout cells compared to fork associated proteins.

d-f, Co-IP experiments performed with antibodies against BRG1 **(d)**, BAF47 **(e)**, BAF170 **(f)** in isogenic Calu6 models for RPA complexes.

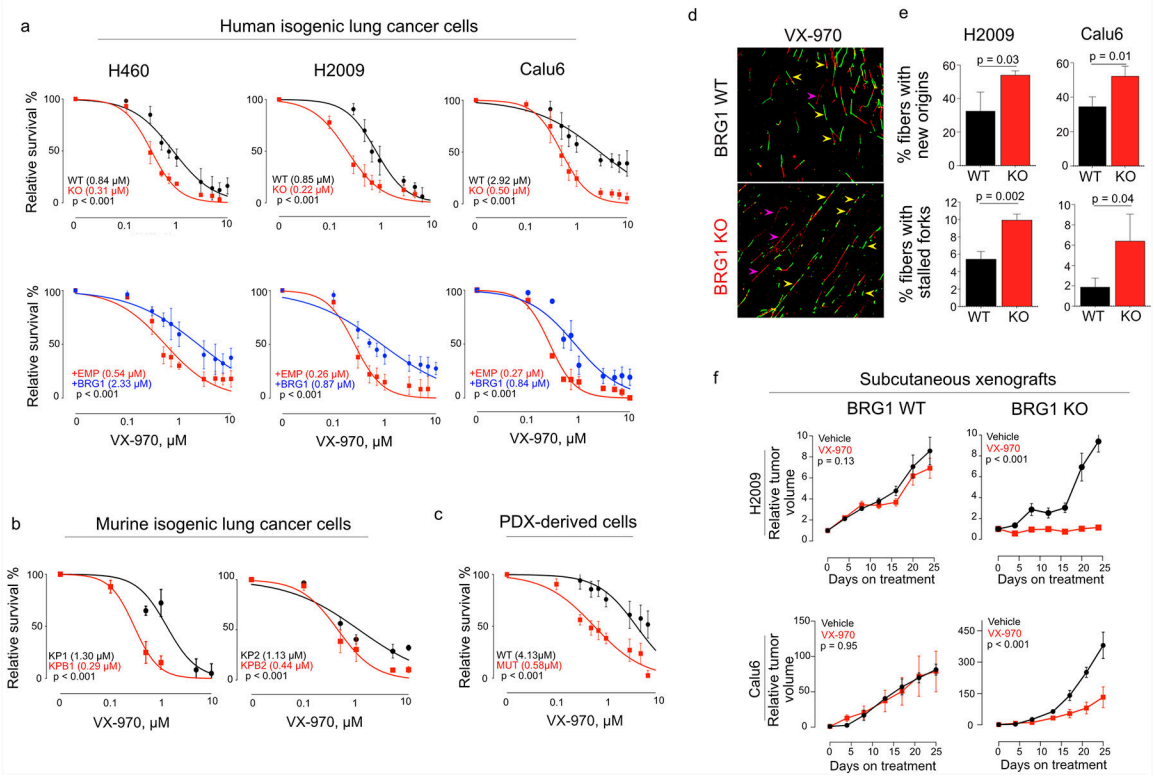

Figure 5. In vitro and in vivo sensitivity of BRG1-mutant lung cancers to ATR inhibition.

a-c, Relative survival in isogenic human **(a)** BRG1 wildtype, knockout, and BRG1 reconstituted cells, **(b)** murine isogenic models of Brg1 loss, and PDX models **(c)** after treatment with increasing doses of ATR inhibitor VX-970 performed for 72 hours using cell-titer glo assays. All data points are relative to vehicle controls. (n = 4–8 for each human cell line, n= 3–5 for each murine cell line, n = 7 for each PDX cell line).

d,e, Representative images of DNA fiber spreads and analysis in human isogenic models of BRG1 loss after ATR inhibition. New origins of replication and fork stalls/collapse are shown by yellow and pink arrowheads, respectively. All images to scale and data is mean ± SD. (n = 3 for each cell line)

f, Subcutaneous tumor volumes of isogenic human BRG1 wildtype and knockout cells after treatment with vehicle or VX-970 for 25–30 days. Average tumor volume ± SEM was measured every 4 days. (H2009; n = 4 (wildtype), n = 3–5 (knockout). Calu6; n = 3 (wildtype), n= 4–6 (knockout)). Two-way ANOVA was performed to compute statistical significance.

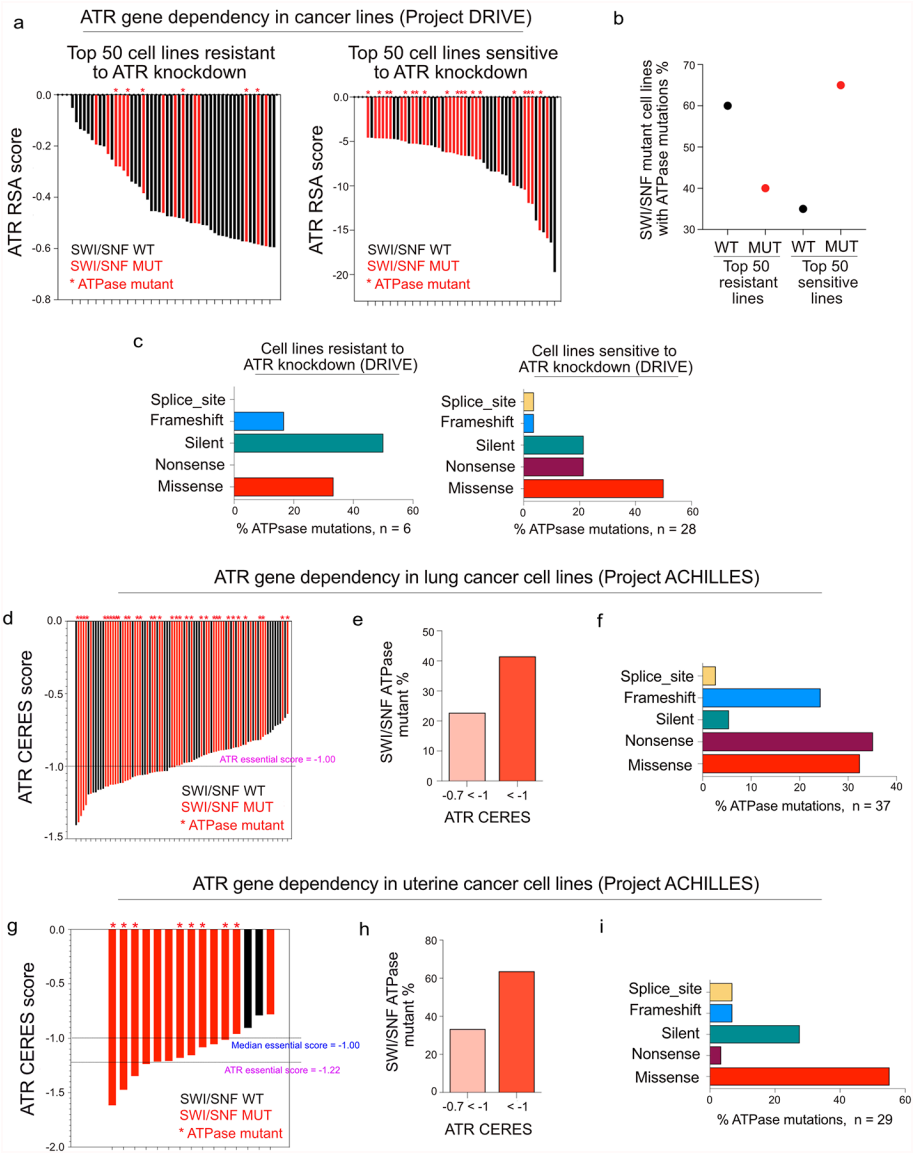

Figure 6. Cancer dependency maps confirm synthetic lethal relationship between BRG1 and ATR.

a-c, Analysis of siATR RSA scores from Project DRIVE. Types of ATPase mutations identified in cancer lines.

d-i, Analysis of ATR knockout CERES scores from Project ACHILLES in lung **(d-f)** and uterine **(g-i)** cancer cell lines. ATR CERES range less than −0.7 are depicted (lung, **e**; uterine, **h**). 37 SWI/SNF ATPase mutations (lung, **f**) and 29 (uterine, **i**) were identified in this analysis and have been grouped according to mutation type.